Chapter 1

Introduction

1.1 Massive star formation

1.1.1 What are massive stars?

Stars are the "atoms" of our universe. By mass, they are classified as low-mass stars ($M \sim 0.05 - 2\ M_\odot$), intermediate-mass stars ($M \sim 2 - 8\ M_\odot$), and, the major focus of this thesis, massive stars ($M \geq 8\ M_\odot$) which are defined by their mass exceeding the Chandrasekhar limit (core mass $\sim 1.4\ M_\odot$), so that during their death with catastrophic core collapse they become neutron stars ($M \sim 8 - 25\ M_\odot$) or black holes ($M > 25\ M_\odot$). Unlike low-mass stars, which dominate the stellar population, massive stars are relatively rare, according to the high-mass end (about $\geq 1\ M_\odot$) of the initial mass function (IMF; Salpeter 1955; Kroupa 2001; Chabrier 2003, see Bonnell et al. (2007) for more discussion) formulated as

$$\frac{dN}{dM} \propto M^{-2.35}, \tag{1.1}$$

or

$$\frac{dN}{d\log M} \propto M^{-1.35}, \tag{1.2}$$

where dN is the number count per mass bin dM. The Salpeter IMF implies that for a stellar population with massive stars, most of the mass is in low-mass stars (total mass $\sim \int M dN$), while most of the luminosity comes from massive stars (assuming[1] $L \propto M^3$, total luminosity $\sim \int L dN$). Therefore, the rare massive stars can influence the evolution of interstellar medium (ISM), galaxies, and our universe. In Table 1.1, we classify main-sequence massive stars by their mass or spectral type. In this thesis, we focus on the early B-type to late O-type stars. The rarity of these stars can be seen in Table 1.1 if the IMF follows Eq. (1.1).

[1] c.f. Salaris & Cassisi (2005) for stellar mass greater than about 2 $M_\odot$

Table 1.1. Classification of main-sequence massive stars

Mass	Designation	Spectral Type	N[a]
8–16 $M_\odot$	early B-type	B3V to B0V	17
16–32 $M_\odot$	late O-type	O9V to O6V	7
32–64 $M_\odot$	early O-type	O5V to O2V	3
64–128[b] $M_\odot$	O/WR-tpye	WHL–H	1

Note. — Adopted from Table 1 and Table 2 of Zinnecker & Yorke (2007). [a]Number of stars according to the initial mass function $dN/dM \sim M^{-2.35}$ if the number count of the highest mass range is normalized to unity. [b] A more realistic upper limit of this mass range is $\sim 150\ M_\odot$ (Figer 2005).

Although rare, massive stars are the main factories that synthesize atoms up to iron during their main-sequence lifetime and produce heavier elements during their supernova phase. This ISM enrichment is a very fast process at cosmic timescales since the typical lifetime of a massive star is only a few Myrs. Within this short period, massive stars provide strong feedback to the ISM through intense and massive outflows, dissociative UV radiation, powerful stellar winds, expanding HII regions, and supernova explosions. A combination of this feedback provides a source of turbulence[2] in the ISM of galaxies, which is thought to be an important mechanism controlling star formation (McKee & Ostriker 2007) and galaxy evolution (Kennicutt & Evans 2012).

1.1.2 Where are the birthplaces of massive stars?

The birthplaces of massive stars may be found by looking at the location of the end-product of their formation — the main sequence OB stars. OB stars are found in clusters and associations (Blaauw 1991; Lada & Lada 2003; Portegies Zwart et al. 2010), which are different in size scales ($\sim 1-10$ pc for clusters, and $\sim 10-100$ pc for associations). Note that OB star clusters can also be members of OB associations. If the current morphology of the two distributions does not change much due to dynamical interactions of stars after their formation, the different size scales imply that massive star formation can happen at very different scales in molecular clouds (relatively local or global). One interesting finding is that in clusters, massive stars are usually located near the center and

[2]Extraction of ordered kinetic energy from galactic rotation, mediated via spiral density waves or cloud collisions is also a possible source of turbulence (e.g., Tan 2000; Tasker & Tan 2009).

surrounded by numbers of lower-mass stars (e.g, Hillenbrand & Hartmann 1998). This mass segregation in clusters again implies that either massive stars tend to be directly formed near the densest part of cluster-forming cores (Bonnell & Davies 1998), or they are formed first in parts of clusters and cascade down to the center by dynamical relaxation (Binney & Tremaine 1987).

Clusters containing massive stars can have very different total stellar masses and numbers of OB stars, likely linked to the total masses of the original molecular clouds (Williams & McKee 1997). For example, the probability of finding a single O9.5 star in a cloud with mass of $10^5\ M_\odot$ is about 50%. If the cloud mass is $10^6\ M_\odot$, it is highly probable to form at least one late O-type star. The nearest cluster containing O-type stars is the Orion Nebula Cluster (ONC) at distance of 414 ± 7 pc (Menten et al. 2007). Its total stellar mass is about $10^3\ M_\odot$, including a few O-type stars. NGC 3603 (in the Carina region at $\sim$ 7 kpc) with about a few dozen O-stars and R136 (in the 30 Doradus region in Large Magellanic Cloud at 55 kpc) with a few hundred O-stars are other examples of massive clusters, which have stellar masses of 10^4 and $10^5\ M_\odot$, respectively. It is expected that their original cloud masses must be higher by one or two orders of magnitude.

There is a third type of massive star that is not found in either clusters or associations, but in the field. From observations, de Wit et al. (2004, 2005) conclude that about 50% of field massive stars can be directly traced back to nearby OB clusters or associations. They are dynamically ejected with velocities more than 40 km s^{-1} from the regions where they formed (e.g., Blaauw 1961). Typical proper motions of OB stars are only a few km s^{-1}. However, the birthplace of a few % of known field OB stars cannot be identified, leading to the question of how they formed in field. A remarkable example is the O9.5 star HD93521, which is located at $\sim$ 1 kpc above the galactic plane and is believed to have formed in the galactic halo (Irvine 1989). In the 30 Doradus region of Large Magellanic clouds, the evidence of isolated massive star formation is also found (Bressert et al. 2012). To understand this, the formation of massive stars in clusters and (relative) isolation needs to be uncovered.

1.1.3 How do massive stars form?

Compared to the formation of their low-mass counterparts, our understanding of the formation and early evolution of massive stars is still sketchy (Zinnecker & Yorke 2007; Beuther et al. 2007). We begin with an outline of the stages of low-mass star formation and later point out the main differences and difficulties for massive star formation. Followed by the observational classification of massive star-forming cores, we outline possible scenarios of massive star formation.

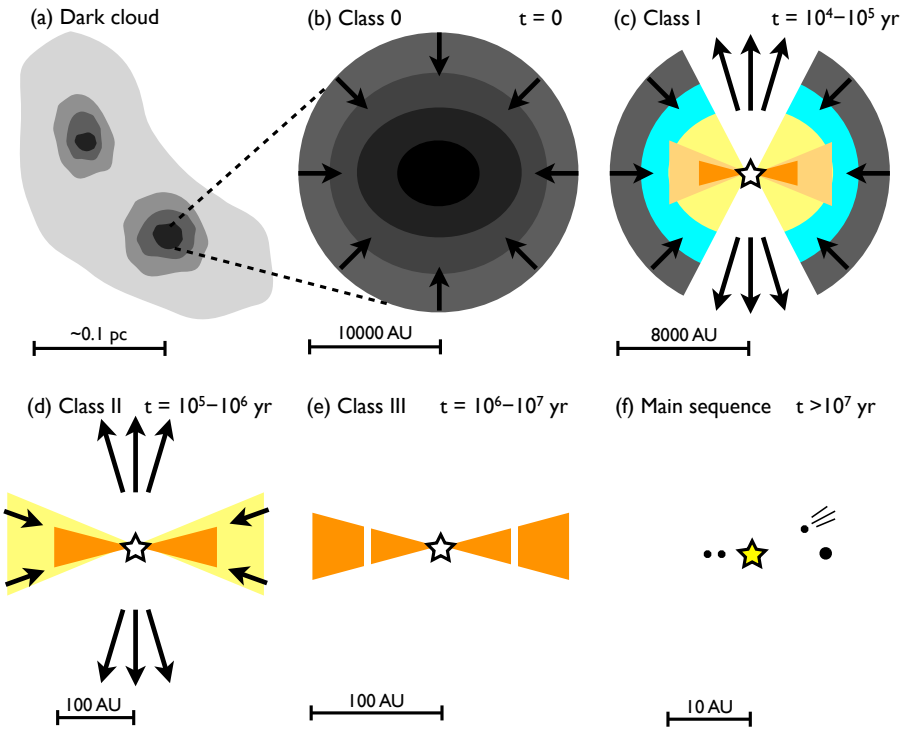

Figure 1.1 Evolutionary stages of low-mass star formation.

1.1.3.1 Low-mass star formation

For an isolated low-mass star, the formation process is summarized by Shu et al. (1987) and McKee & Ostriker (2007) and is presented graphically by Wilking (1989) (Fig. 1.1). Low-mass star formation happens in dense cores (size: 0.03-0.2 pc, density: 10^{4-5} cm^{-3}) of molecular clumps (size: $\sim 0.3 - 3$ pc, density: 10^{3-4} cm^{-3}) embedded in dark molecular clouds (size: $\sim 2 - 15$ pc, density: 50–500 cm^{-3}; Bergin & Tafalla 2007, and reference therein). The temperature reaches its local minimum of $\sim$ 10 K for a prestellar core before global infall. Once gravitational collapse happens (Class 0), the core is heated inside-out and may drive a high temperature chemistry with rich emission from complex organic molecules (e.g., the hot corino: IRAS 16293–2422; Kuan et al. 2004; Bottinelli et al. 2004; Bisschop et al. 2008; Caux et al. 2011; Jørgensen et al. 2011). The conservation of angular momentum of infalling cores results in the formation of circumstellar disks in Keplerian rotation (Class I or eariler). At this stage, mass transfer happens from envelope to disk and then from disk to star, while in the meantime the excess of angular momentum can be removed via bipolar outflows. Most of the final stellar mass is acquired at this stage (accretion timescale $t_{\rm acc} \sim$

few $\times 10^5$ yr; Evans et al. 2009). In a later less embedded phase with little mass transfer from any remaining envelope to disk (Class II), a pre-main-sequence star is surrounded by a protoplanetary disk and may still be driving a weak bipolar outflow. Later, the bipolar outflow ceases and the pre-main-sequence star contracts slowly toward the main sequence (Class III). Typical timescales of 10^7 yr for contraction of a low-mass protostar are estimated via the Kelvin-Helmholtz time,

$$t_{\rm KH} = \frac{GM^2}{RL}, \tag{1.3}$$

where M, R, and L are stellar mass, radius, and luminosity, respectively. Therefore, for low-mass star formation, $t_{\rm acc}$ is smaller than $t_{\rm KH}$, meaning that there is a well-defined pre-main sequence phase. The total amount of time to form a mature planetary system, like our Solar system, from the onset of the collapse of prestellar core is more than 10^7 yr. The formation time of a low-mass star is about 0.1% of its total lifetime.

1.1.3.2 Massive star formation: difficulties

The difficulties of massive star formation come from the fact that forming massive stars are not only rare (according to the IMF) but they evolve very fast over $\sim 10^5$ yr or a few % of their total lifetime (few 10^6 yr; Churchwell 2002) while still highly embedded ($A_V > 100$ mag). Most importantly, the Kelvin-Helmholtz time for massive stars is only $10^4 - 10^5$ yr, meaning that massive stars enter the main sequence phase while collapse of the dense core and subsequent accretion still happen. A distinct difference between low- and high-mass star formation is that massive stars generate intense and dissociative UV radiation, leading to radiation pressure that is strong enough to halt accretion and generate HII regions. Early studies show that if massive stars form through spherical accretion, an upper-limit on the stellar mass of $\sim 40\ M_\odot$ is found (highly depends on dust properties; Kahn 1974; Wolfire & Cassinelli 1987), which also sets a cutoff to the IMF. However, from observations, a cutoff of about 150 $M_\odot$ is more likely (e.g., Figer 2005), implying that formation schemes other than spherical accretion must exist. Through 2D axi-symmetric simulations following massive star formation from a collapsing core to an accretion disk including radiation feedback, Yorke & Sonnhalter (2002) found that the radiation problem is less severe since the disk in the equatorial plane around the forming massive star helps to redirect the stellar radiation to the polar direction allowing accretion in the equatorial regions (see also Nakano et al. 1995; Jijina & Adams 1996). This is the so-called "flashlight effect". The cavities created by bipolar outflows also enhance the flashlight effect (Krumholz et al. 2005b). Radiation may not always be destructive since massive stars may form through radiatively driven Rayleigh-Taylor instabilities (Krumholz et al. 2005a). Alternatively, the radiation problem

can be solved by introducing a high accretion rate of the order of 10^{-3} to 10^{-4} $M_{\odot}$ yr^{-1} which is high enough to sustain inward motion (McKee & Tan 2003). We note that if massive stars form through accretion, the requirement of high accretion rates is implicitly implied by their short lifetime. The high accretion rates also enable accretion through ionized flows (Keto 2007).

Our understanding of massive star formation is not only limited by theoretical difficulties, but also by observational limits. Massive star-forming regions are typically at a few kpc from our Sun, thus high-angular resolution observations are required. Apart from their distance, massive star-forming cores are highly embedded, which only centimeter, millimeter, submillimeter, and mid/far-infrared wavelengths can penetrate. In addition, the rapid evolution of massive star-forming cores makes the target selection difficult. The mixture of stellar feedback and high column densities of star-forming materials make the interpretation of observational data non-straightforward.

1.1.3.3 Massive star formation: observational phases

Although it is difficult to observe massive star-forming regions, modern techniques at the above mentioned wavelengths allow us to classify massive star-forming cores observationally (Churchwell 1999; Beuther et al. 2007; Zinnecker & Yorke 2007). In the following, we highlight the various components of this classification one by one, as shown in Fig. 1.2.

High-mass starless core (Fig. 1.2 a)

Massive star formation starts in high mass starless cores (HMSC) within molecular clumps where the density reaches a local maximum ($> 10^6$ cm^{-3}) and the temperature is a local minimum (< 20 K). The typical masses of these clumps, with typical sizes of 0.25–0.5 pc, are a few 100 to a few 1000 $M_{\odot}$ (e.g., Beuther et al. 2002a; Williams et al. 2004). The mean density is about 10^5 cm^{-3}. Infrared Dark Clouds (IRDC), identified as dark filaments against bright infrared backgrounds (Simon et al. 2006), are one type of objects that satisfy the above conditions. High-mass starless cores are rare, suggesting that their timescales may be very short (e.g., Ragan et al. 2012).

High-mass protostellar object (Fig. 1.2 b)

This type of source is classified based on the detection of infall signatures, non-detection of cm-wave emission from ionized gas, and non-detection or weak detection of emission from complex molecules. The absence of free-free emission indicates that the forming stars have not yet reached the limit for hydrogen fusion. The forming stars may be still low-mass to intermediate-mass. The non-detection of the emission from complex molecules may be due to limited sensitivity of observations, since the hot core is still small in size. Hot dense gas confined close to forming stars is expected to be present inside any HMPO.

Hot molecular core (Fig. 1.2 c)

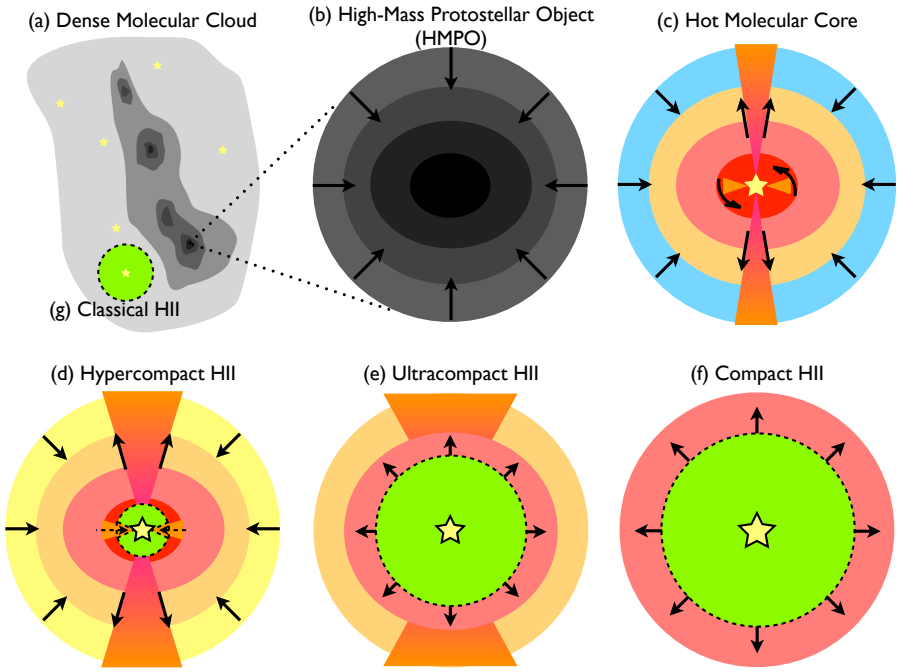

Figure 1.2 Observational classification of massive star-forming cores.

This type of source is characterized by its rich emission from complex organic molecules such as CH_3OH, $HCOOCH_3$, and C_2H_5CN, etc. (e.g., Kurtz et al. 2000; Cesaroni 2005), as an indication that a significant part of the star-forming core has been heated up, leading to evaporation of ice on dust grains and further high-temperature gas-phase chemistry (Herbst & van Dishoeck 2009).

Hypercompact and ultracompact HII regions (Fig. 1.2 d and e)
Once the forming massive stars start fusion at their central regions, the intense UV radiation can ionize the surrounding gas, leading the formation of hypercompact or ultracompact HII regions (Kurtz 2005; Hoare et al. 2007). The difference between the two is their size. Typical sizes are few 100 AU to few 1000 AU. These small HII regions are spatially confined to their host stars. Hypercompact HII regions are suggested as the remnant of photoevaporating disks (Keto 2007), while ultracompact HII regions contain no disk and photoionize their surrounding molecular cocoon.

Compact and classical HII regions (Fig. 1.2 f and g)
Ionization happens globally (pc scales) in these type of sources (Mezger et al. 1967; Yorke 1986). They expand hydrodynamically and disrupt the parent molecular cloud. At this stage, embedded massive stars with their surrounding low-mass stellar population can be observed at optical and near infrared wavelengths.

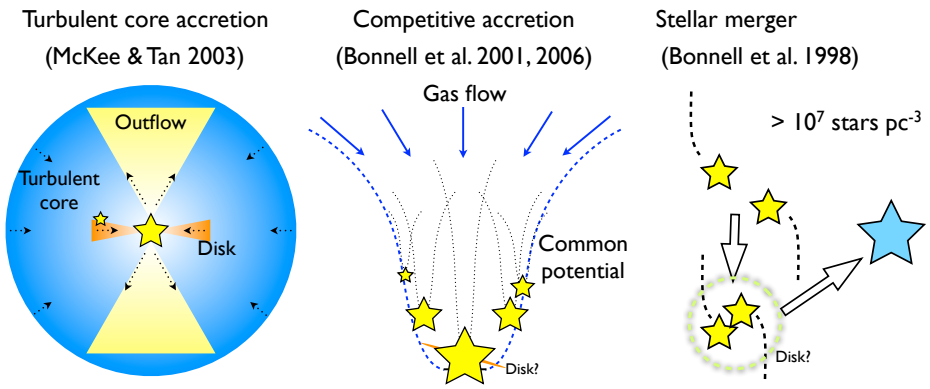

Figure 1.3 Theories of massive star formation.

The above observationally defined classes of objects may be linked in an evolutionary ordering. We note that the sequence presented in Fig. 1.2 does not necessarily represent one according to evolution. In fact, the evolution of a forming massive star is so fast that it is hard to construct a distinct evolutionary sequence and it is observationally difficult to distinguish evolution from luminosity differences. The above different phases may be coexisting. A possible formation sequence of a single massive star or a small cluster may be as follows: HMPO (Fig. 1.2 (b)), hypercompact HII (Fig. 1.2 (d)), ultracompact HII (Fig. 1.2 (e)), compact HII (Fig. 1.2 (f)), and classical HII (Fig. 1.2 (g)). The hot molecular core phase (Fig. 1.2 (c)) may coexist with hypercompact and ultracompact HII regions.

1.1.3.4 Massive star formation: theories

The formation of massive stars may follow two very different scenarios: by accretion, or by coalescence (merger). The latter model provides a brute-force solution to avoid the radiation problem by allowing direct collision of stellar components in dense clusters (Bonnell & Davies 1998). The former can be further classified into two different accretion mechanisms: turbulent core accretion (McKee & Tan 2003) and competitive accretion (Bonnell et al. 2001; Bonnell & Bate 2006). These three different concepts of massive star formation are summarized in Fig. 1.3.

The turbulent core accretion model or monolithic collapse model is similar to the formation of isolated low-mass stars as outlined in Sect. 1.1.3.1, but with modification in the strength of turbulence and accretion rates. In this model, core density and velocity dispersion follow power-laws as functions of radius. The turbulence is strong enough to provide ram pressure to support the core against fragmentation before massive star formation proceeds. The star-forming

core can also be supported by large-scale magnetic fields. The high accretion rates ($10^{-4} - 10^{-3}$ $M_{\odot}$ yr^{-1}) are able to sustain accretion in an environment with strong radiation pressure. Accretion can proceed through a disk, which also helps to redirect radiation in the polar direction. The final stellar mass is correlated with the initial mass of the star-forming core. In other words, the accretion happens locally. The overall picture of massive star formation resembles its low-mass counter part. (i.e., a collapsing core with formation of a disk and outflows)

Competitive accretion relies on the physics of gravity and the observational fact that massive stars usually form in clustered environments. The initial star-forming cloud (pc scales) does fragment down to thermal Jeans mass ($\approx 1\ M_{\odot}$). For regions with higher (proto)stellar density, further run-away growth can proceed by Bondi-Hoyle accretion (Bondi 1952), which describes the accretion process of a spherical object traveling in the interstellar medium, or tidal accretion enabled by the joint gravitational potential of star clusters. The relatively massive stars (not necessarily yet $> 8\ M_{\odot}$) sitting at the bottom of the joint gravitational potential well have the highest chance to become more massive stars ($> 8\ M_{\odot}$). Accretion happens globally at cloud scales down to core scales (i.e., the mass for a given massive star may come from any part of the parent cloud and depends on how the infalling material is distributed over the most massive cluster members). In addition, this type of formation mechanism is able to reproduce the full IMF similar to the observed one (Bonnell et al. 2007).

The most dramatic mechanism of forming a massive star is through coalescence of lower-mass protostars or main sequence stars in the center of dense clusters with stellar densities higher than $\sim 10^7$ pc^{-3}. This merger scenario is a violent process during which circumstellar disks will be destroyed, outflows will be disrupted, and stars may be ejected.

1.1.4 Why do kinematics at small scales (≤ 0.1 pc) matter?

Among the three dominant theories of massive star formation, disks and outflows are essential components, but with different properties. In the turbulent core accretion model, these structures are more long-lived, while in the other two formation schemes, these structures should be perturbed and likely short-lived. The high occurrence of collimated massive bipolar outflows observed toward massive star-forming cores (Zhang et al. 2001; Beuther et al. 2002b) provides a strong hint that the formation of massive stars may follow the disk accretion process similar to the turbulent core accretion model. However, to date, the presence of circumstellar "disks" is reported only toward about few tens or so young early B-type stars, via (sub)millimeter observations (summarized by Cesaroni et al. 2007) and direct imaging in infrared wavelengths (e.g., Kraus et al. 2010; Boley et al. 2012). These disk-like structures are found to be large ($\sim 10^{2-4}$ AU)

and massive ($M_{\rm disk} \leq M_\star$), which is quite different from the disks around low-mass protostars ($M_{\rm disk} \ll M_\star$). On the contrary, only large "toroids" undergoing solid-body rotation with masses greater than stellar masses are found toward young O-type stars (e.g., Beltrán et al. 2005; Furuya et al. 2008). These rotating structures show diverse characteristics. Therefore, it is interesting to study massive star-forming cores on small scales (≤ 0.1 pc scales) with high-angular resolution observations and focus on the gas motions including turbulence, infall, outflow, and especially *rotation*. Furthermore, the presence of disks open up the possibility of planet formation around massive stars.

1.2 Methodology

1.2.1 Millimeter and submillimeter observations

Observations at millimeter and submillimeter wavelengths are important in the field of star formation. At these wavelengths, cold and warm dust can be probed by measuring its thermal emission. Physical conditions, such as temperature, density, kinematics, as well as chemical conditions, such as chemical abundances and distributions, can be studied through rotational transitions of interstellar molecules. With the advent of millimeter and submillimeter interferometric facilities such as the Submillimeter Array (SMA), Combined Array for Millimeter Astronomy (CARMA), and Plateau de Bure interferometer (PdBI), it is now possible to investigate the physical and chemical conditions of massive star forming cores on small scales in detail. Interferometric observations are especially important for hunting for massive disks since typical massive star-forming regions are located at a few kpc from the Sun and the typical sizes of massive disks are a few 1000 AU or less, corresponding to $\sim 1''$ or less.

The basic idea of (sub)millimeter interferometry is that instead of building a single huge single element telescope to achieve high angular resolution following $\theta_{\rm HPBW} \sim \lambda/D$, where $\theta_{\rm HPBW}$ is the half-power beam width, λ is the observing wavelength, and D is the size of the dish, a set of small dishes is distributed over an area and linked together to simulate an equivalent big single-dish telescope. The signal from the sky is correlated for each pair of antennas, with the correction of the geometric delay and instrumental delay. At an instantaneous moment, different pairs of antennas have different spatial sensitivity formulated as $\theta_{ij} \sim \lambda/B_{ij}$, where θ_{ij} is the spatial resolution for a given antenna pair ij, and B_{ij} is the length of the baseline ij. Due to the Earth rotation, the spatial sensitivity of each baseline changes due to the projection effect. An ensemble of different correlations with different projections forms a spatial sampling in the Fourier plane or (u,v) plane. In principle, samples with small uv-distances ($\sqrt{u^2+v^2}$) probe signal from large scales, while samples with large uv-distances are more sensitive to signal from small scales. We note that uv-data or "visibility" data

are the real output from interferometers, not direct images. Images are reconstructed by performing Fourier transformation of the visibility and subsequent image processing.

Although through interferometric techniques, high angular resolution can be obtained at (sub)millimeter wavelengths, there are caveats. The largest spatial sensitivity is set by the smallest uv sampling. Therefore, interferometers are blind to signals coming from scales greater than the scales set by the shortest baselines. This is the so-called "missing flux" problem. This potential problem may be solved by filling the uv gap with single dish (total power) observations. So far, full image synthesis (combining single-dish and array data) is still not a routine observing strategy. In this thesis, we use both single dish observations and (sub)millimeter interferometric observations to individually study the gas kinematics of massive star-forming cores at different scales.

1.2.2 Observing dust emission and molecular line emission

Dust and molecules are essential components of star-forming cores. At a temperature of 10–100 K, dust is a strong emitter at (sub)millimeter wavelengths. By measuring its continuum emission, one can estimate the total dust mass of the source by assuming a dust temperature and a dust opacity. Ossenkopf & Henning (1994) provides a good reference of dust opacities for star-forming cores. With an additional assumption on the gas-to-dust ratio, one can also derive the total H_2 mass and column density of the source.

Molecular transitions are classified in terms of electronic transitions, vibrational transitions, and rotational transitions. The former two transitions correspond to UV/optical and mid-infrared wavelengths, respectively. Rotational transitions of molecules mainly fall in the (sub)millimeter wavelength regime. The physical conditions associated with star-forming regions are especially suitable for excitation of rotational levels of molecules. By measuring molecular rotational emission lines, one can estimate the physical and chemical conditions of the star-forming cores. In addition, molecular lines carry kinematical information. Therefore, observing molecular lines at (sub)millimeter wavelengths is well suitable to probe infall and rotation near forming massive stars.

Hot molecular cores are associated with massive star-forming regions (Sect. 1.1.3.3). The evaporation of icy mantles from the surfaces of dust grains plus high-temperature gas-phase reactions result in rich complex organic molecules. The first model of hot core chemistry was proposed by Brown et al. (1988) who followed the gas-phase chemistry of cold gas during the core collapse, including the accretion and subsequent surface reactions on dust grains, until the heating mechanism drives the icy mantles back to the gas phase. Later Charnley et al. (1992) demonstrated that a realistic mixture of ices containing H_2O, NH_3 and CH_3OH, as observed in cold clouds, could reproduce the observed molecular

abundances in the Orion KL hot molecular core by high temperature chemistry following evaporations. The hot core chemistry has been further extended to include S-bearing (Charnley 1997), Si-bearing (Mackay 1995) and P-bearing (Charnley & Millar 1994) species. Because of new insights into gas phase chemistry, however, more recent models suggest that most of the complex molecules are formed on the grain surfaces (Garrod & Herbst 2006). As the result of rapid change of physical conditions in massive star-forming regions, chemical ingredients could be classified into three kinds: (1) molecules which are formed in the pre-collapse phase and released from the icy mantles on dust grains (e.g., C_2H_2, CO); (2) molecules that are made on the surface of dust grains and released back to gas phase (e.g., NH_3, CH_3OH); and (3) molecules that are formed in the gas phase after mantle evaporation. Hot core observations are thus important to provide constraints on the chemical ingredients both in the gas phase and solid phase of hot core models. In this thesis, we utilize the emission from hot core molecules as the diagnostics of physical conditions including kinematics.

1.2.3 Radiative transfer and molecular excitation

The signal from the sky observed by telescopes is described by the equation of radiative transfer,

$$\frac{dI_\nu}{dz} = -\kappa_\nu I_\nu + j_\nu, \tag{1.4}$$

where I_ν is the specific intensity, z is the coordinate system along the line of sight, κ_ν is the absorption coefficient and j_ν is the emission coefficient (Fig. 1.4). Both κ_ν and j_ν are macroscopic parameters. Microscopically, these two parameters are related to the atomic or molecular properties. The microscopic interplay between radiation and matter is conveniently described by the Einstein coefficients A and B. Collisions, determined by temperature and density, happen between particles and are described by the collisional rate coefficient C. Here we focus on the rotational transitions of interstellar molecules, which millimeter and submillimeter observations are sensitive to. Every molecule has its own unique "pattern" of discrete energy levels based on quantum theory (c.f., Townes & Schawlow 1955). For simplicity, we assume a two-level system (Fig. 1.4). This two-level system can be de-excited via spontaneous emission, stimulated emission, and collisions with transition probabilities of $A_{\rm ul}$, $\frac{4\pi}{c} I_\nu B_{\rm ul}$, and $n_{\rm col} C_{\rm ul}$ respectively, while the system can be excited via absorption of radiation and collision with transition probabilities of $\frac{4\pi}{c} I_\nu B_{\rm lu}$ and $n_{\rm col} C_{\rm lu}$, respectively ($n_{\rm col}$ is the volume density of the collisional partner). The observed spectral lines are the results of detailed balance between radiation and collision, and the integration over the emitting medium along the line of sight based on the radiative transfer equation (Eq. 1.3).

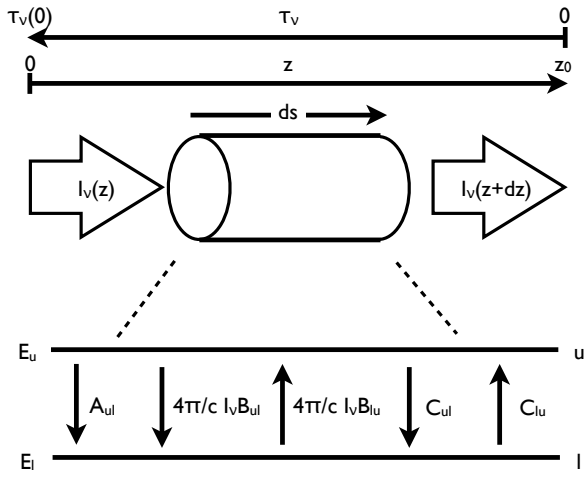

Figure 1.4 A sketch of radiative transfer process including molecular excitation.

In general, solving the equation of radiative transfer to understand the excitation conditions for a given molecule is a complicated task (van der Tak 2011). This requires good assumptions of temperature, density, and velocity distribution, as well as source geometry. Most importantly, the collisional rate coefficients of molecules are needed, which so far have been tabulated for only few molecules and limited levels (c.f., Schöier et al. 2005). However, it is still possible to derive some basic quantities, such as excitation temperature $T_{\rm ex}$ and total molecular column density $N_{\rm tot}$, from the observed line intensities, without solving the radiative transfer equation. The most straightforward and frequently used method is the "rotation diagram" (e.g., Turner 1991), which assumes that the observed transitions are all optically thin and follow a single Boltzmann distribution at $T_{\rm ex}$. If the observed target has high enough gas density to fully thermalize the energy levels via collisions, the derived $T_{\rm ex}$ is a good approximation of the kinetic temperature ($T_{\rm kin}$). If, however, some transitions are optically thick, or the energy levels are subthermally excited, this method results in highly uncertain $T_{\rm ex}$ as well as $N_{\rm tot}$. For molecules with known collisional rate coefficients, this problem may be solved by using approximated methods to solve to detailed balance of energy levels and radiative transfer, such as the large velocity gradient (LVG) approximation (Goldreich & Kwan 1974) or escape probability method (Rybicki 1985). In this thesis, we use the computer program RADEX (van der Tak et al. 2007) to perform this type of analysis. This approach still assumes that the source is homogeneous and characterized by a single $T_{\rm kin}$, a single $N_{\rm tot}$, and an uniform gas density. To fully solve the equation of radiative transfer including detailed balance of energy levels as a function of space with varying temperature

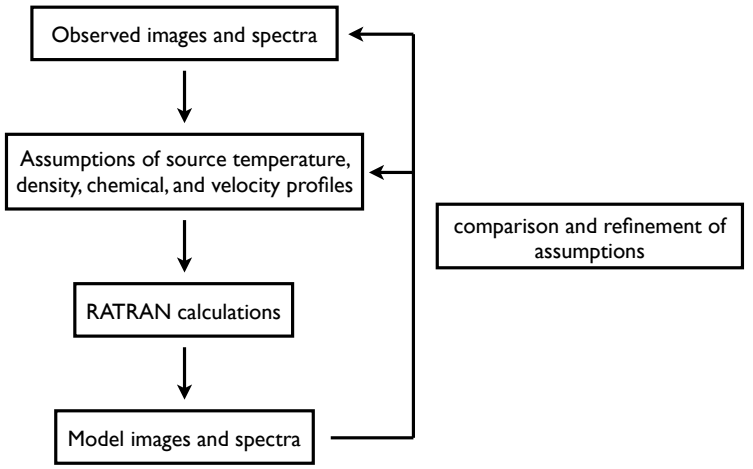

Figure 1.5 Steps of radiative transfer modeling of kinematics with RATRAN.

and density, we utilize the state-of-art code RATRAN (Hogerheijde & van der Tak 2000), which employs an accelerated Monte Carlo approach.

1.2.4 Radiative transfer modeling of kinematics

In this thesis, we mainly focus on the observed molecular line profiles which carry kinematical information of massive star-forming cores. Although a molecular transition has a well defined transition frequency ($\nu = (E_{\rm u} - E_{\rm l})/h$, with h the Planck constant), the observed line profile is usually not a delta function. The finite width of the observed line profiles is a superposition of many aspects. Due to the uncertainty principle of quantum theory, the line is broadened naturally. This effect, however, is negligible for rotational lines, compared to thermal Doppler broadening, which is the result of thermal random motion. In the warm ($\geq$ 100 K) massive star-forming cores, the thermal linewidth is about a few 0.1 km s^{-1} only. The typical broad linewidth (few to several km s^{-1}) observed toward massive star-forming cores implies that non-thermal Doppler broadening effects, such as motions like infall, outflow, rotation, and turbulence, dominate the observed line profiles. To extract the kinematical information hidden in the observed line profiles, we use the radiative transfer code RATRAN (Hogerheijde & van der Tak 2000) as an engine to generate model line profiles with the above non-thermal motions and compare with observations. In Fig. 1.5, we visualize the steps of RATRAN modeling of the kinematics. The analysis of the kinematics in this thesis is performed on a qualitative basis, limited by the data.

1.3 Components of this thesis

In this thesis, the diagnostics provided by molecular line emission and dust emission are used to understand the physical conditions associated with massive star-forming cores at various scales (few 100 AU to few 10000 AU). Kinematics on these scales is the focus of this work. In the following chapters, one survey and three case studies are presented.

1.3.1 Chapter 2

In this chapter, we present single-dish observations with the James Clerk Maxwell Telescope (JCMT) toward 17 massive star-forming cores in lines of $C^{17}O$, $C^{34}S$, and CH_3CN near 345 GHz. We aim to establish if these species are indeed robust tracers of disks as suggested by interferometric observations in the literature. We compare the observed spectra with generic radiative transfer models including infall, rotation, and turbulence to have an idea on the origin of the observed linewidth. We conclude that $C^{17}O$ 3–2 best traces turbulence at scales of a few 10000 AU, while $C^{34}S$ mainly traces turbulence at scales of a few 1000 AU. CH_3CN 18–17 lines are the best disk tracer at 1000 AU scales or less, compared to the other two transitions. Further detailed radiative transfer modeling of individual sources is required to disentangle these single-dish line profiles. This chapter will be submitted to A&A.

1.3.2 Chapter 3

In this chapter, we present interferometric observations with the Submillimeter Array (SMA) at 354 GHz toward the proto-Trapezium cluster forming region W3 IRS5. The $1''$–$3''$ resolution continuum and line data allow us to study the structure, kinematics, and chemistry at 2000–6000 AU scales. The continuum observations show five emission peaks with two forming massive stars and the other three as either starless cores or low-mass star-forming cores with the potential to become massive stars in the future. The kinematics are found to be very complex in the clustered environment of W3 IRS5. From this dataset, we suggest that the proto-Trapezium cluster W3 IRS5 is an ideal test case to discriminate between models of massive star formation. Either the massive stars accrete locally from their local cores; in this case the small core masses imply that W3 IRS5 is at the very end stage ($\sim$1000 yr) of infall and accretion. Alternatively, the stars may be still accreting from the global collapse of a massive, cluster forming core. Observations that reliably probe infall from large to small scales are needed answer this question. This chapter is published in A&A, 2013, 558, A69.

1.3.3 Chapter 4

In this chapter, we present arcsecond to subarcsecond resolution interferometric observations with the Plateau de Bure interferometer (PdBI) in the 1.3 mm and 3 mm bands toward a forming late O-type star AFGL 2591–VLA3. Through radiative transfer modeling of the HDO $1_{1,0}$–$1_{1,1}$ and $H_2{}^{18}O$ $3_{1,3}$–$2_{2,0}$ line profiles, we propose that there is a layered disk-like structure undergoing subKeplerian rotation and radial expansion around AFGL 2591–VLA3. The subKeplerian motion may be due to magnetic braking in the disk regions, while the expansion may be the signature of outflow or disk wind activities. Our observations imply that late O-type stars may form following the turbulent core accretion model. This chapter is published in A&A, 2012, 543, A22.

1.3.4 Chapter 5

In this chapter, we present subarcsecond resolution interferometric observations with the expanded Submillimeter Array (eSMA) at 345 GHz in both molecular lines and dust continuum toward the early B-type star S255IR–SMA1. The 345-GHz continuum of SMA1 is resolved at $\sim 0.3''$ resolution (500 AU) for the first time. We find that massive star formation activity is highlighted by the presence of the emission from complex hot core molecules. In addition, a disk-like structure is found in CH_3OH lines which shows a clear velocity gradient perpendicular to large scale outflows. Through a comparison with radiative transfer models, the observed velocity gradient cannot be characterized by Keplerian rotation with the expected stellar mass. Through luminosity analysis, we find that S255IR–SMA1 is a young ($10^3 - 10^4$ yr) forming early B-type star with a high accretion rate (few 10^{-4} $M_\odot$ yr^{-1}). Our observations also act as supporting evidence that an early B-type star may form following the turbulent core accretion scenario. This chapter is submitted to A&A.

1.4 General conclusion and Outlook

In this section, we highlight our general conclusions drawn from chapters 2 to 5 of this thesis. The central goal of this thesis is to characterize the kinematics of massive star-forming cores at scales of 0.1 pc or less. We especially focus on the properties of the rotational component, i.e., massive disks, in massive star-forming cores. Through single-dish and interferometric observations at millimeter and submillimeter wavelengths, we conclude:

(1) $C^{17}O$ 3–2 and $C^{34}S$ 7–6 are good tracers of turbulence in massive star-forming cores at scales of a few 10000 AU and a few 1000 AU, respectively. Typical turbulent linewidths are $\sim$2–4 km s^{-1} at these scales, suggesting that massive star-forming cores are highly turbulent. (Chapter 2)

(2) Hot core molecules such as CH_3OH and CH_3CN, are good lines to hunt for disks at scales of $\sim$ 1000 AU or less around massive forming stars. (Chapter 2 and 5)

(3) Hot core molecules are good tracers for massive star formation activity. (Chapter 2, 3, and 5)

(4) Late O-type stars may also form through disk accretion. (Chapter 4)

(5) Fossil molecules, such as deuterated species which formed in the cold prestellar phase, are potentially good probes for rotation in massive star-forming cores. (Chapter 4)

(6) Around very young forming early B-type stars, disks may not be Keplerian. Magnetic fields at scales of few 100 AU may regulate the kinematics of the disk. (Chapter 5)

(7) Supporting evidence for the turbulent core accretion model and the competitive accretion model is found in our case studies. (Chapter 3, 4, and 5)

With the main conclusions outlined above, we will continue our hunt for massive disks with the Atacama Large Millimeter/sub-millimeter Array (ALMA). Its superior sensitivity at subarcsecond resolution is the best tool for this research. With ALMA, the speed of hunting for massive disks can be boosted by factors of 10–100, compared to current (sub)millimeter interferometers. Sensitive line observations are essential for detailed radiative transfer modeling with better constraints. Wideband line observations are also very powerful to select potential good disk tracers in an uniform way. We believe that ALMA can provide answers to the ultimate question of this thesis: how do massive stars form?

Bibliography

Beltrán, M. T., Cesaroni, R., Neri, R., et al. 2005, A&A, 435, 901

Bergin, E. A. & Tafalla, M. 2007, ARA&A, 45, 339

Beuther, H., Churchwell, E. B., McKee, C. F., & Tan, J. C. 2007, Protostars and Planets V, 165

Beuther, H., Schilke, P., Menten, K. M., et al. 2002a, ApJ, 566, 945

Beuther, H., Schilke, P., Sridharan, T. K., et al. 2002b, A&A, 383, 892

Binney, J. & Tremaine, S. 1987, Galactic dynamics

Bisschop, S. E., Jørgensen, J. K., Bourke, T. L., Bottinelli, S., & van Dishoeck, E. F. 2008, A&A, 488, 959

Blaauw, A. 1961, Bull. Astron. Inst. Netherlands, 15, 265

Blaauw, A. 1991, in NATO ASIC Proc. 342: The Physics of Star Formation and Early Stellar Evolution, ed. C. J. Lada & N. D. Kylafis, 125

Boley, P. A., Linz, H., van Boekel, R., et al. 2012, A&A, 547, A88

Bondi, H. 1952, MNRAS, 112, 195

Bonnell, I. A. & Bate, M. R. 2006, MNRAS, 370, 488

Bonnell, I. A., Bate, M. R., Clarke, C. J., & Pringle, J. E. 2001, MNRAS, 323, 785

Bonnell, I. A. & Davies, M. B. 1998, MNRAS, 295, 691

Bonnell, I. A., Larson, R. B., & Zinnecker, H. 2007, Protostars and Planets V, 149

Bottinelli, S., Ceccarelli, C., Neri, R., et al. 2004, ApJ, 617, L69

Bressert, E., Bastian, N., Evans, C. J., et al. 2012, A&A, 542, A49

Brown, P. D., Charnley, S. B., & Millar, T. J. 1988, MNRAS, 231, 409

Caux, E., Kahane, C., Castets, A., et al. 2011, A&A, 532, A23

Cesaroni, R. 2005, in IAU Symposium, Vol. 227, Massive Star Birth: A Crossroads of Astrophysics, ed. R. Cesaroni, M. Felli, E. Churchwell, & M. Walmsley, 59–69

Cesaroni, R., Galli, D., Lodato, G., Walmsley, C. M., & Zhang, Q. 2007, Protostars and Planets V, 197

Chabrier, G. 2003, ApJ, 586, L133

Charnley, S. B. 1997, ApJ, 481, 396
Charnley, S. B. & Millar, T. J. 1994, MNRAS, 270, 570
Charnley, S. B., Tielens, A. G. G. M., & Millar, T. J. 1992, ApJ, 399, L71
Churchwell, E. 1999, in NATO ASIC Proc. 540: The Origin of Stars and Planetary Systems, ed. C. J. Lada & N. D. Kylafis, 515
Churchwell, E. 2002, ARA&A, 40, 27
de Wit, W. J., Testi, L., Palla, F., Vanzi, L., & Zinnecker, H. 2004, A&A, 425, 937
de Wit, W. J., Testi, L., Palla, F., & Zinnecker, H. 2005, A&A, 437, 247
Evans, II, N. J., Dunham, M. M., Jørgensen, J. K., et al. 2009, ApJS, 181, 321
Figer, D. F. 2005, Nature, 434, 192
Furuya, R. S., Cesaroni, R., Takahashi, S., et al. 2008, ApJ, 673, 363
Garrod, R. T. & Herbst, E. 2006, A&A, 457, 927
Goldreich, P. & Kwan, J. 1974, ApJ, 189, 441
Herbst, E. & van Dishoeck, E. F. 2009, ARA&A, 47, 427
Hillenbrand, L. A. & Hartmann, L. W. 1998, ApJ, 492, 540
Hoare, M. G., Kurtz, S. E., Lizano, S., Keto, E., & Hofner, P. 2007, Protostars and Planets V, 181
Hogerheijde, M. R. & van der Tak, F. F. S. 2000, A&A, 362, 697
Irvine, N. J. 1989, ApJ, 337, L33
Jijina, J. & Adams, F. C. 1996, ApJ, 462, 874
Jørgensen, J. K., Bourke, T. L., Nguyen Luong, Q., & Takakuwa, S. 2011, A&A, 534, A100
Kahn, F. D. 1974, A&A, 37, 149
Kennicutt, R. C. & Evans, N. J. 2012, ARA&A, 50, 531
Keto, E. 2007, ApJ, 666, 976
Kraus, S., Hofmann, K.-H., Menten, K. M., et al. 2010, Nature, 466, 339
Kroupa, P. 2001, MNRAS, 322, 231
Krumholz, M. R., Klein, R. I., & McKee, C. F. 2005a, in IAU Symposium, Vol. 227, Massive Star Birth: A Crossroads of Astrophysics, ed. R. Cesaroni, M. Felli, E. Churchwell, & M. Walmsley, 231–236
Krumholz, M. R., McKee, C. F., & Klein, R. I. 2005b, ApJ, 618, L33
Kuan, Y.-J., Huang, H.-C., Charnley, S. B., et al. 2004, ApJ, 616, L27
Kurtz, S. 2005, in IAU Symposium, Vol. 227, Massive Star Birth: A Crossroads of Astrophysics, ed. R. Cesaroni, M. Felli, E. Churchwell, & M. Walmsley, 111–119
Kurtz, S., Cesaroni, R., Churchwell, E., Hofner, P., & Walmsley, C. M. 2000, Protostars and Planets IV, 299
Lada, C. J. & Lada, E. A. 2003, ARA&A, 41, 57
Mackay, D. D. S. 1995, MNRAS, 274, 694
McKee, C. F. & Ostriker, E. C. 2007, ARA&A, 45, 565
McKee, C. F. & Tan, J. C. 2003, ApJ, 585, 850

Menten, K. M., Reid, M. J., Forbrich, J., & Brunthaler, A. 2007, A&A, 474, 515
Mezger, P. G., Altenhoff, W., Schraml, J., et al. 1967, ApJ, 150, L157
Nakano, T., Hasegawa, T., & Norman, C. 1995, ApJ, 450, 183
Ossenkopf, V. & Henning, T. 1994, A&A, 291, 943
Portegies Zwart, S. F., McMillan, S. L. W., & Gieles, M. 2010, ARA&A, 48, 431
Ragan, S., Henning, T., Krause, O., et al. 2012, A&A, 547, A49
Rybicki, G. B. 1985, in Progress in stellar spectral line formation theory, p. 199 - 206, ed. J. E. Beckman & L. Crivellari, 199–206
Salaris, M. & Cassisi, S. 2005, Evolution of Stars and Stellar Populations
Salpeter, E. E. 1955, ApJ, 121, 161
Schöier, F. L., van der Tak, F. F. S., van Dishoeck, E. F., & Black, J. H. 2005, A&A, 432, 369
Shu, F. H., Adams, F. C., & Lizano, S. 1987, ARA&A, 25, 23
Simon, R., Jackson, J. M., Rathborne, J. M., & Chambers, E. T. 2006, ApJ, 639, 227
Tan, J. C. 2000, ApJ, 536, 173
Tasker, E. J. & Tan, J. C. 2009, ApJ, 700, 358
Townes, C. H. & Schawlow, A. L. 1955, Microwave Spectroscopy
Turner, B. E. 1991, ApJS, 76, 617
van der Tak, F. 2011, in IAU Symposium, Vol. 280, IAU Symposium, ed. J. Cernicharo & R. Bachiller, 449–460
van der Tak, F. F. S., Black, J. H., Schöier, F. L., Jansen, D. J., & van Dishoeck, E. F. 2007, A&A, 468, 627
Wilking, B. A. 1989, PASP, 101, 229
Williams, J. P. & McKee, C. F. 1997, ApJ, 476, 166
Williams, S. J., Fuller, G. A., & Sridharan, T. K. 2004, A&A, 417, 115
Wolfire, M. G. & Cassinelli, J. P. 1987, ApJ, 319, 850
Yorke, H. W. 1986, ARA&A, 24, 49
Yorke, H. W. & Sonnhalter, C. 2002, ApJ, 569, 846
Zhang, Q., Hunter, T. R., Brand, J., et al. 2001, ApJ, 552, L167
Zinnecker, H. & Yorke, H. W. 2007, ARA&A, 45, 481